RSC Advances

ROYAL SOCIETY OF CHEMISTRY

www.rsc.org/advances

Controllable Hydrothermal-assisted Synthesis of Mesoporous Co_3O_4 Nanosheets

Xiulan Hu [a,*], Huihong Huang [a,#], Jianbo Zhang [a], Junjun Shi [a], Shoufeng Zhu [a], Nan Su [a]

[a] College of Materials Science and Engineering, Nanjing Tech University, China

* Corresponding author at: College of Materials Science and Engineering, Nanjing Tech University, Xin-Mo-Fan Road No. 5, Nanjing, Jiangsu 210009, China.

Tel./fax: +86 25 8358 7260.

E-mail address: whoxiulan@163.com (X. Hu).

Huihong Huang and Xiulan Hu are co-first authors.

Abstract: Mesoporous cobalt oxide (Co_3O_4) nanosheets (about 15 nm in thickness and about 1 μm in width) with mostly pore size of 10 ~ 15 nm were obtained by heat treatment of hydrothermal-synthesized hydrothermal products at 300 °C. The compositions and morphologies of hydrothermal products could be tailored by controlling hydrothermal reaction temperature at a range of 120 °C ~ 200 °C and time. Quasi-sheet-like $Co(OH)_2$ favors to form at 120 °C for 6 h through the oriented attachment, and then slice sheets $Co(NH_3)_5(ONO)(NO_3)_2$ and $Co(CN)_2{\cdot}H_2O$ were formed at over 150 °C for 6 h in water due to thermodynamic instability. Their sheets become thinner and more decentralized with the extension of hydrothermal reaction time. And $(CH_3COO)_2Co$ precursor were hydrothermal synthesized in ethanol. All of hydrothermal products were transformed into porous Co_3O_4 with similar morphologies after heat treatment. Mesoporous Co_3O_4 nanosheets displayed a

Brunauer-Emmett-Teller (BET) surface area of about 65 m^2g^{-1}. Cyclic voltammetry (CV) results indicated mesoporous Co_3O_4 nanosheets have good electrochemical property and show a specific capacitance (C_S) of 880 Fg^{-1} in 1 M KOH at a current density of 1 Ag^{-1}.

Keywords: Cobalt oxide; Synthesis; Hydrothermal method; Mesoporous; Nanosheets; Electrochemical property

1. Introduction

Normal spinel (AB_2O_4) structured Co_3O_4 nanomaterials were widely used in various fields, such as CO, CH_4 gas catalytic oxidation,[1-3] biological cell sensors,[4-6] supercapacitor[7-9] and lithium air batteries[10-12] or lithium ion batteries[13-15] because of its good catalytic and electrochemical properties.

Presently, a controllable preparation of cobalt oxide nanoparticles has attracted much attention because particles size and morphology have an important influence on their properties and applications. Moreover, a great number of research projects have been focused on exploring efficient synthetic routes to obtain size- and morphology-controllable cobalt oxide nanomaterials during the past few years.[16, 17]

Homogeneous nanostructured Co_3O_4 with different morphologies like hierarchical sphere,[18-20] octahedron,[21, 22] plates,[23, 24] nanorods,[25-27] nanowires,[4, 28], nanotubes[29, 30], nanocubes[17, 31, 32] and nanosheets[33-36] are synthesized via various methods such as molten salt method, pyrolytic process, sol-gel method, microwave method, electrodeposition method and hydrothermal method.

Among of these methods, hydrothermal method is an essential and powerful approach toward fabricating nanomaterials at low temperature due to its maneuverability and large-scale fabrication.[37] Until now, even though Co_3O_4 nanoparticles can be synthesized directly by hydrothermal method, most of them are cube shape or particles.[38-40] Therefore, in order to obtain cobalt oxide with a high specific surface and excellent property, cobalt oxide is currently almost gotten by two steps, which are synthesis of hydrothermal products with various morphologies by hydrothermal method and subsequently thermal decomposition of hydrothermal products. For instance, Ying et al.[41] fabricated mesoporous Co_3O_4 hierarchical nanobundles by thermal treatment of a complex hydrothermal products, which were synthesized via hydrothermal method at 180 °C for 12 h. Generally, cobalt hydroxide and cobalt carbonate are two popular hydrothermal products because of their ease of synthesis and stable at hydrothermal conditions (100 °C to 180 °C). For examples, Xie et al.[42] synthesized layered Co_3O_4 nanomaterials from $Co_2(OH)_2CO_3$ using nitrate hexahydrate and polyvinyl pyrrolidone. Pan and co-workers[43] synthesized free-standing mesoporous Co_3O_4 nanodiscs with about 20 nm in thickness and 200 nm in width from $Co(OH)_2$. And Tu's group[44] synthesized porous Co_3O_4 nano-potato-fakes with 10 nm in thickness on Ni foam substrate at 100 °C by a nitrate-salt-mediated formation route to prepare α-$Co(OH)_2$ as hydrothermal products. These nanofakes are generally perpendicular to the substrate and interconnected with each other to form a highly open net-structure. And cobalt oxide sheets (with about 20 nm in thickness and 200 nm in width) were synthesized.[24, 43] The above results

clarified templates is necessary. Thus it is difficult to obtain large-size and monodispersed Co_3O_4 without template [36, 45- 47] or surfactant through a simple hydrothermal method until now.[48]

As it well known, urea[42, 49, 50] and NaOH[24, 43] are usually utilized as precipitating reagents under hydrothermal conditions. However, surfactants or templates are necessary to obtain controlled morphology.[43, 44, 49, 50] From the viewpoint of environmental protection and practicality, it is better to develop a simple, environment-benign and large-scale route to synthesize Co_3O_4 nanomaterials without using any additives of surfactants or templates. Recently hexamethylenetetramine (HMT), which can generate hydroxyl ions through decomposition at more than 70 °C, was used to synthesize porous ZnO nanosheets without using any surfactants or templates during the synthesis process.[51]

So far, there are many reports on the synthesis of Co_3O_4 nanosheets including using electrodeposition, hydrothermal and direct precipitation. But most of them took electrodeposition to synthesis Co_3O_4 nanosheets on a selected substrate (such as nickel foam). [33, 35, 52] And although Co_3O_4 nanosheet arrays were synthesized using hydrothermal method, but it also needs to grow on a nickel substrate. [36, 47] Herein in this study, we aim to substrate-free obtain monodispersed mesoporous Co_3O_4 nanosheets by controllable hydrothermal products from a reaction system of cobalt nitrate hexahydrate and hexamethylenetetramine. The effects of reaction parameters (such as hydrothermal temperature and time, and solvent) on composition and morphology of hydrothermal products are discussed in detail. And formation

mechanism of hydrothermal products and electrochemical property of mesoporous Co_3O_4 nanosheets are investigated, too.

2. Experimental

2.1 Synthesis of mesoporous Co_3O_4 nanosheets

All chemicals of cobalt nitrate hexahydrate ($Co(NO_3)_2 \cdot 6H_2O$, Aladdin, 99.9%), hexamethylenetetramine ($C_6H_{12}N_4$, Ling feng chemical reagent, Shanghai Co., Ltd, 99.9%), ethanol (C_2H_5OH, Ya sheng chemical reagent, Wuxi Co., Ltd, 99.9%) were used as purchased without further purification. In a typical synthesis, 0.005 mol $Co(NO_3)_2 \cdot 6H_2O$ and 0.008 mol $C_6H_{12}N_4$ were dissolved into 75 mL distilled water. After stirring for 30 min at room temperature, the resulting mixture solution was transferred into a 100 ml Teflon-lined stainless-steel autoclave to maintain at a given temperature range of 100 °C to 200 °C for 1~24 h. Subsequently, all precipitates were separated from solution by centrifugation and washing with distilled water for several times. The clean precipitates were dried in air at 80 °C for 6 h. Finally, hydrothermal-synthesized precipitates were heat treated at 300 °C for 3 h at a heating rate of 2 °C/min to yield Co_3O_4 in order to keeping original nanosheet morphology of hydrothermal products avoiding sintering deformation according to previous experimental results as shown in Fig. S1.† And ethanol served as the solvent, a similar synthesis process was investigated, too.

2.2 Characterization

Phase compositions of all products were analyzed by powder X-ray diffraction (XRD, Rigaka Smartlab) with Cu Kα (λ=1.5418 Å) incident radiation at 30 kV

voltage and 40 mA current. XRD patterns were recorded from 5 to 85 ° (2θ) with a scanning step of 8 °/min. The size, morphology and microstructure of products were observed by a field emission scanning electron microscopy (FE-SEM, HITACHI S4800) and a transmission electron microscopy (TEM, JEM-2100F). The specific surface area of mesoporous Co_3O_4 was measured by a Brunauer-Emmett-Teller (BET, ASAP 2020) method using nitrogen adsorption and desorption isotherms on a micromeritics instrument corporation sorption analyze.

2.3 Electrochemical measurements

Cyclic voltammetry (Zennium Electrochemical workstation, Germany) was applied to evaluate electrochemical properties of Co_3O_4 nanoparticles using a three-electrode system consisting of a glassy carbon working electrode (GCE, ϕ= 3 mm, geometrical area of 0.07 cm^2), a platinum rod counter electrode (ϕ= 1 mm), and an Ag/AgCl reference electrode (saturated with 3.5 M KCl aqueous). The working electrode was prepared as the follows: a 2 mL ethanol-suspension solution including Co_3O_4 nanoparticles were obtained by ultrasonic dispersion for 30 min with 6 μL of 5% Nafion aqueous. A droplet (8 μL) of well-mixed ethanol-suspension solution was placed on a surface of clean glassy carbon electrode and kept up to dryness at room temperature. Cyclic voltammetry was performed in an aqueous 1 M KOH solution. The working electrode was cycled between 0 and 0.6 V at a scan rate of 20 mV/s.

For characterization of capacitor property, Co_3O_4 electrodes were fabricated on cleaned nickel foam substrates. First, nickel foam was cleaned in 1 M HCl for 15 min, and subsequently washed in water and ethanol for 5 min each. A required amount of

active materials (mesoporous Co_3O_4 nanosheets) were mixed with polyvinylidenefluoride (PVDF) (HSV900, Altuglas, France) and acetylene black (Yi Bo Rui regent, Tianjing Co., Ltd) in the weight ratio of 80:15:5 in N-methyl-2-pyrrolidinone (Da Mao reagent, Tianjing Co., Ltd) for better homogeneity. Then as-prepared slurry was pasted onto a cleaned nickel foam substrate (area ~1 cm^2) and dried in an oven at 60 °C for 12 h. And the dried electrode was pressed using a hydraulic press at a pressure of about 10 MPa. Mass loading of the active materials was about 3 mg. Electrochemical properties of mesoporous Co_3O_4 nanosheets were studied by galvanostatic charge-discharge cycling in 1 M KOH electrolyte in three-electrode configuration.

3. Results and discussion

The XRD result as shown in Fig. 1a confirmed Co_3O_4 was prepared by thermal decomposition of hydrothermal products obtained at 180 °C for 6 h in water. All diffraction peaks are well agree with the standard card of Co_3O_4 (JCPDS card No.42-1467, space group Fd3m). No peaks of any other phases were detected.

SEM image of Co_3O_4 as shown in Fig. 1b clarified that Co_3O_4 are monodispersed and mesoporous nanosheets (Fig. S3†). The cross section image of nanosheets is well-presented with a thickness of about 15 nm and width of 1 μm as shown in Fig. 1b and its inset. The size of as-prepared mesoporous Co_3O_4 nanosheets are much larger than that of as-previous reported Co_3O_4 hexagonal nanosheets (with a thickness of 10~20 nm and width of 50~200 nm).[24, 43, 53, 54] Commonly, such mesoporous Co_3O_4 nanosheets are resulted from hydrothermal products and their thermal decomposition.

Thus it is necessary to controllable synthesis of hydrothermal products. The formation mechanism of hydrothermal products will be discussed in later.

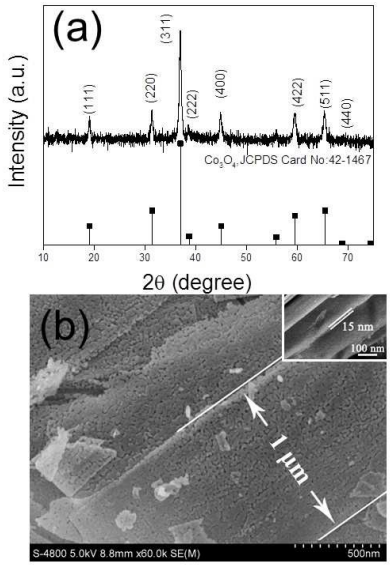

Fig. 1 X-ray diffraction pattern (a) and SEM image (b) of mesoporous Co_3O_4 nanosheets. The inset in (b) is a cross-section SEM image of nanosheets.

Fig. 2 (a, b) shows typical TEM images for a mesoporous Co_3O_4 nanosheet. The mesoporous nanosheets consist of a large amount of pores. The mostly pore sizes are about 10 ~ 15 nm. And there are parts of connected pore leading to the formation of big holes. These pores are derived from the removal of NH_3, ONO^-, NO_3^- CN^- and H_2O species by thermal decomposition from cobalt hydrothermal products of cobalt ammine nitrate nitrite ($Co(NH_3)_5(ONO)(NO_3)_2$,JCPDS card No.49-1125) and cobalt cyanide hydrate ($Co(CN)_2{\cdot}H_2O$, JCPDS card No.24-0327) as shown in latter Fig. 4c and 4d. As previously reported, pores of most Co_3O_4 nanosheets are common derived from the removal of OH^- small species by thermal decomposition from cobalt hydroxide.[34, 53, 54] The high resolution TEM image as shown in Fig. 2c clearly indicate

Co_3O_4 quasi-sheet-like nanomaterials have good crystallinity with a lattice spacing value of 0.24 nm, which agrees with the (311) planes of Co_3O_4. The good crystallinity is also confirmed by selected area electron diffraction (SAED) pattern (Fig. 2d), which is in agreement with the XRD result.

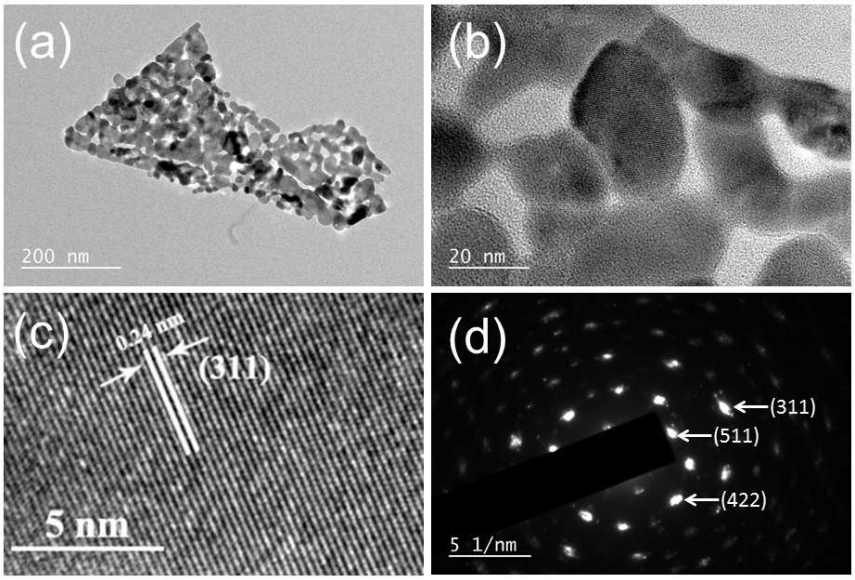

Fig. 2 A typical TEM image of a mesoporous Co_3O_4 nanosheet (a) and (b), high resolution TEM image (c) and SAED pattern (d) of mesoporous Co_3O_4.

Fig. 3 shows a nitrogen adsorption-desorption isotherms of mesoporous Co_3O_4 nanosheets. The nitrogen adsorption-desorption isotherms display a type IV isotherm having a large hysteresis loop at a pressure range of 0.6~1.0 P/P_0, suggesting the presence of mesoporous in Co_3O_4 nanosheets. Moreover, when the relative pressure is close to 1, the amount of adsorbed N_2 rapidly increases, indicating that macroporous also exist in Co_3O_4 nanosheets. Such mesoporous and macroporous were considered to derive from the release of gases (CO_2, NO_2 and H_2O) from cobalt hydrothermal products of $Co(NH_3)_5(ONO)(NO_3)_2$ and $Co(CN)_2 \cdot H_2O$ during thermal decomposition

process. Using the Brunauere Emmette Teller (BET) method, the surface area of mesoporous Co_3O_4 nanosheets is measured to be about 65 m^2g^{-1}.

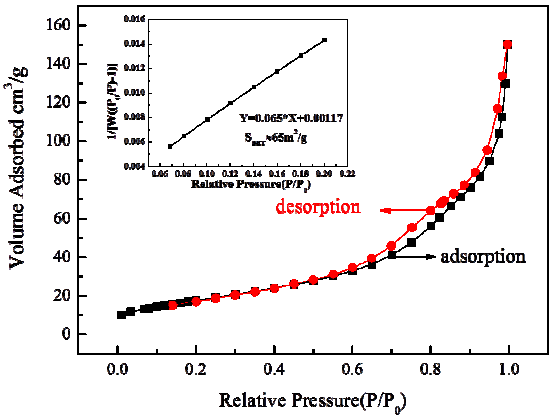

Fig. 3 Nitrogen adsorption-desorption isotherms of mesoporous Co_3O_4 nanosheets.

As the above discussed, Co_3O_4 morphologies are dependent upon those of hydrothermal products. In order to controllable synthesize hydrothermal products, we have studied the effect of hydrothermal temperature and time on hydrothermal products in detail.

Fig. 4 show XRD patterns of as-prepared hydrothermal products from cobalt nitrate hexahydrate and hexamethylenetetramine by hydrothermal method at the range of 100 °C to 300 °C for 6 h. An unknown intermediate with two characteristic diffraction peaks was detected at 100 °C for 6 h (Fig. 4a). It should be due to very slow reaction rate because $C_6H_{12}N_4$ began to release of OH^- at more than 70 °C. And then cobalt hydroxide ($Co(OH)_2$, JCPDS card No.49-1125) were detected at 120 °C because of high OH^- concentration (Fig. 4b). In dynamics, $Co(OH)_2$ were easily formed and relatively stable at low temperature. But when temperature increased up

to 150 °C, $Co(OH)_2$ was a thermaldynamic instability phase and favored to transform to $Co(NH_3)_5(ONO)(NO_3)_2$ and $Co(CN)_2{\cdot}H_2O$ (Fig. 5c). And their intensities of diffraction peaks obviously became strong when temperature was increased up to 200 °C. While once temperature was increased up to 300 °C, about 1~3 μm cube-shaped Co_3O_4 particles were directly synthesized (Fig. 4e and Fig. S4†). This result was quite different from the results of Hu,[38] side length of cube about 10 nm to about 36 nm. These results clarified $Co(NH_3)_5(ONO)(NO_3)_2$ and $Co(CN)_2{\cdot}H_2O$ are intermediate phases during the process of hydrothermal reaction in an approximate temperature range in the reaction system of cobalt nitrate hexahydrate and hexamethylenetetramine. By the way, pompon-like Co_3O_4 were synthesized if raw materials $Co(NO_3)_2{\cdot}6(H_2O)$ was directly calcinated at 300 °C for 3 h in the air (Fig. S2†).

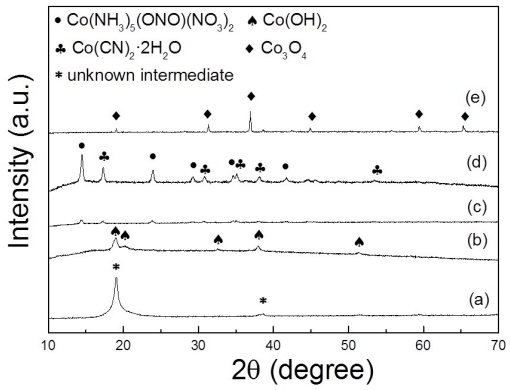

Fig. 4 XRD patterns of as-prepared hydrothermal products at different temperatures for 6 h. (a) 100 °C, (b) 120 °C, (c) 150 °C, (d) 200 °C and (e) 300 °C.

Fig. 5 shows the morphologies of as-prepared hydrothermal products prepared at a temperature range of 100~180 °C nearly looked like sheet. With the increase of

reaction temperature, the sheets became thinner and more decentralized. Taking XRD and FE-SEM results into consideration, we understood that all morphology of $Co(OH)_2$, $Co(NH_3)_5(ONO)(NO_3)_2$ and $Co(CN)_2 \cdot H_2O$ was sheet-like.

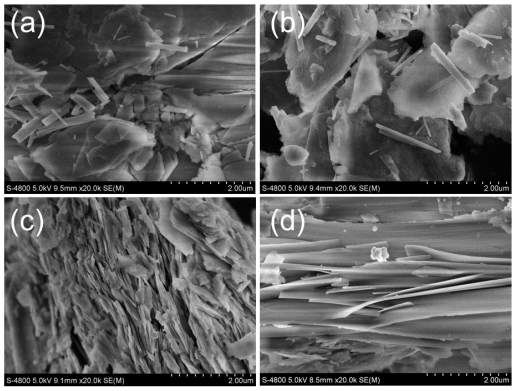

Fig. 5 SEM images of as-prepared hydrothermal products at different temperatures for 6 h: (a) 100 °C; (b) 120 °C; (c) 150 °C and (d) 180 °C.

Moreover, we studied the effect of reaction time on the composition and morphology of hydrothermal products at 150 °C (Fig. 6 and 7). Layered $Co(OH)_2$ was formed for 1 h (Fig. 6a and 7a). When reaction time was extended to more than 6 h, $Co(OH)_2$ readily converted to $Co(NH_3)_5(ONO)(NO_3)_2$ and $Co(CN)_2 \cdot H_2O$ due to thermodynamic instability, and their intensities of all diffraction peaks increased (Fig. 6b~d). And their layers become thinner and more dispersion with increasing reaction time (Fig. 5c and Fig. 7b, c). In addition, it was clear that when the reaction was carried out under stirring, it could improve dispersibility of layers (compared with Fig. 5c and Fig. 8).

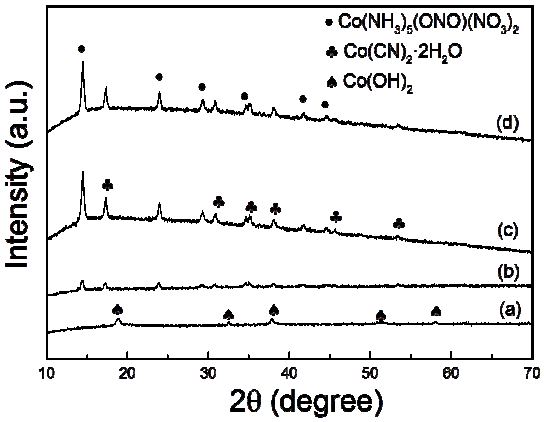

Fig. 6 XRD patterns of as-prepared hydrothermal products at 150 °C for different reaction times. (a) 1 h, (b) 6 h, (c) 12 h and (d) 24 h.

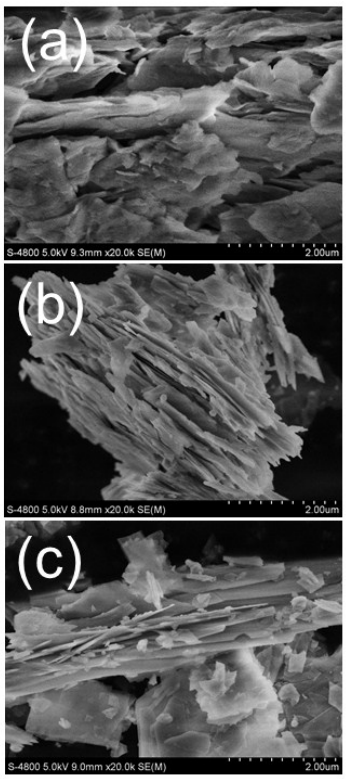

Fig. 7 SEM images of as-prepared hydrothermal products at 150 °C for different times. (a) 1 h, (b) 12 h and (c) 24 h.

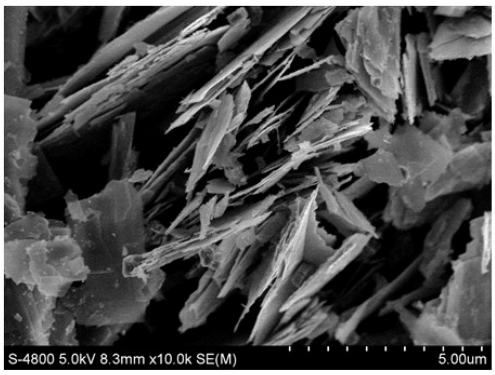

Fig. 8 SEM images of as-prepared hydrothermal products at 150 °C for 6 h with stirring.

Thus compared with the above discussed results, we can speculate that formation mechanism of hydrothermal products under hydrothermal conditions in water as shown in Figure 9. In the initial stage of reaction, the primary $Co(OH)_2$ nanocrystals are formed due to the combination of Co^{2+} and OH^- through gradually decomposition of HMT. Generally, hexagonal $Co(OH)_2$ favors to form via a facile hydrothermal process without a growth substrate. As previously reported, Sun et al. synthesize hexagonal $Co(OH)_2$ by direct precipitation route due to its intrinsic lamellar structure.[34] However in this study, quasi-sheets $Co(OH)_2$ (not hexagonal) favors to form through the oriented attachment and self-assembly due to NH_4^+ and other ions in solution preferred to adsorb on the special facets during growth process (As shown in Fig. 9). And as reaction going on, slice sheets $Co(NH_3)_5(ONO)(NO_3)_2$ and $Co(CN)_2{\cdot}H_2O$ were formed from quasi-sheets $Co(OH)_2$. And their sheets become thinner and more decentralized with the extension of hydrothermal reaction time. Anyway, $Co(NH_3)_5(ONO)(NO_3)_2$ and $Co(CN)_2{\cdot}H_2O$ sheets are unstable to change to

Co_3O_4 at higher hydrothermal temperature. Thus Co_3O_4 was directly synthesized at more than 300 °C under hydrothermal conditions.

The major reactions occurred in water were summarized as following:

$$C_6H_{12}N_4 + 6H_2O \rightarrow 6HCHO + 4NH_3 \quad (1)$$

$$NH_3 + H_2O \rightarrow NH_4^+ + OH^- \quad (2)$$

$$Co^{2+} + 2OH^- \rightarrow Co(OH)_2 \quad (3)$$

$$3Co(OH)_2 + 2HCHO + 12NH_4^+ + 6NO_3^- + 6OH^- \rightarrow 2Co(NH_3)_5(ONO)(NO_3)_2 + Co(CN)_2 \cdot H_2O + 15H_2O \quad (4)$$

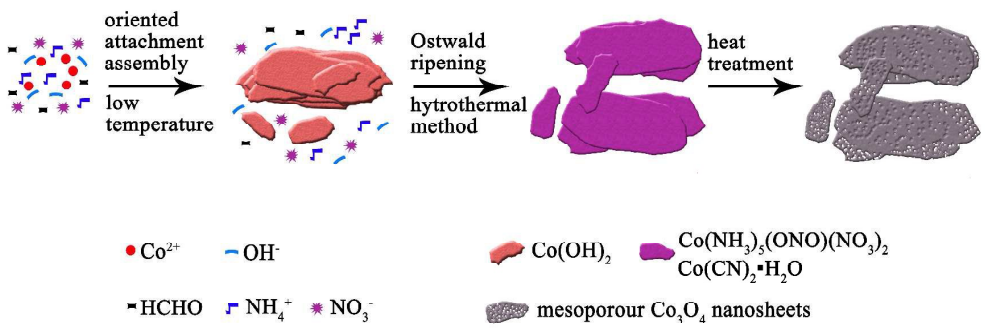

Fig. 9 Schematic illustration for the possible mechanism of mesoporous Co_3O_4 nanosheets.

And we investigated the effects of solvent on composition and morphology of hydrothermal products at 150 °C for 6 h. In the case of ethanol served as a solvent, cobalt acetate hydrate ($(CH_3COO)_2Co \cdot 4H_2O$, JCPDS card No.25-0372) and a small amount of $CoCO_3$ (JCPDS card No.25-0372) was synthesized. And after heat treatment (300 °C for 3 h), hierarchical nanoflowers-like consisted of mesoporous

Co_3O_4 petals (sheet-like) were obtained (Fig. 10a). The morphology was quite different from the result of water as a solvent (Fig. 1b). As we all known, ammonia solubility in the ethanol is much smaller than in the deionized water due to their different polarity. So the variety of solvents influences not only the nucleation of hydrothermal product but also the preferential direction of crystal growth. Therefore, the precursor is $(CH_3COO)_2Co$ in the ethanol system, indicating that ethanol is oxidated into acetic acid during hydrothermal process, and further reacts with Co^{2+}.[4] Noted that irregular shape cobalt oxide particles with different sizes were directly formed if HMT was not added when ethanol served as a solvent (Fig. 10b). As we all know, the oxidizability of Co^{3+} is stronger than COO^-. In the presence of HMT, which has weak reducibility, preferred to oxide alcohol into acetic acid,[55] rather than oxide Co^{2+} into Co^{3+}.

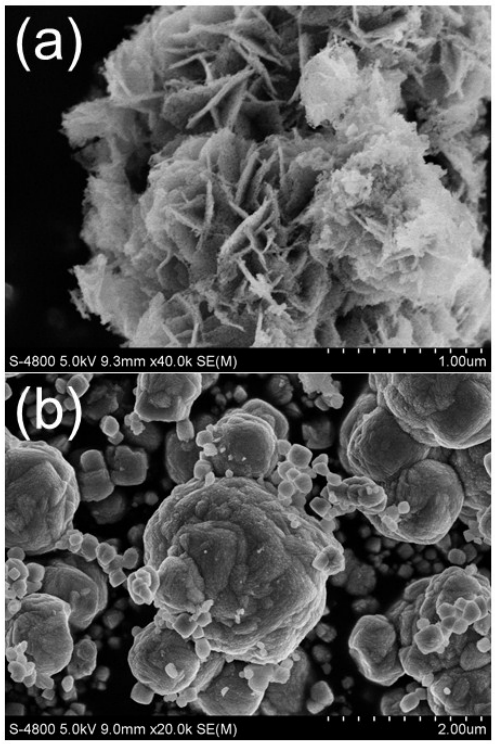

Fig. 10 SEM images of Co_3O_4 prepared in ethanol. (a) with HMT by hydrothermal reaction and further thermal decomposition, (b) without HMT directly by hydrothermal reaction. All hydrothermal reactions were carried at 150 °C for 6 h.

Cobalt oxide, as a kind of promising electrode material, has been utilized in designing and fabricating catalysts, biological cell sensors, supercapacitor and lithium air batteries. Figure 11a shows the electrochemical activity of as-prepared mesoporous Co_3O_4 nanosheets (shown in Fig. 1b) in an aqueous 1 M KOH solution by cyclic voltammetry. A couple of well-defined redox peaks within the potential range from 0 to 0.6 V are clearly observed on the CV curve. The anodic peaks were caused by the conversion of Co (II) and Co (III) to Co (IV) (Eq. (5)). In the reverse sweep, the cathodic peaks belonged to the reduction of Co (IV)/Co (III) and Co (II) (Eq. (5)). It shows good symmetry and reversibility. The good electrochemical property can probably be attributed to the porous structures of Co_3O_4 nanosheets. It has been well addressed that this kind porous structure will be beneficial for improving the electrochemical property because mesoporous are an effective channel of electrons and ions.

$$Co_3O_4 + 4\ OH^- \Leftrightarrow 3CoO_2 + 2H_2O + 4e^- \quad (5)$$

The pseudocapacitive property of mesoporous Co_3O_4 nanosheets electrode were evaluated from the galvanostatic chargeedischarge curves in the voltage range of 0 to 0.5 V in 1 M KOH electrolyte. The first galvanostatic discharge curves at various current densities from which usually practically available C_S of a single electrode is

calculated in Fig. 11b. The discharge curve is observed to be a combination of three processes: (i) a fast initial potential drop followed by (ii) a slow potential decay, and (iii) a faster voltage drop corresponding to electronic double layer capacitor (EDLC).

The C_S was calculated from the charge-discharge curves using the relation, $C_S = (I \cdot t)/(\Delta V \cdot m)$. Where I, t, m and ΔV are applied current, time, active mass, and potential range of the charging and discharging events, respectively. Noted that, our preliminary results clarified the C_S of nickel foam is too little to consider its contribution for electric capacity. Thus the C_S calculated from galvanostatic discharge curves as a function of specific current density (1~10 Ag^{-1}) is in the inset of Fig. 11b. The C_S is 880, 794, 695, and 548 Fg^{-1} at the discharge current density of 1, 2, 5, and 10 Ag^{-1}, respectively. Owing to a large active surface of Co_3O_4 nanosheets is isolated from electrolyte ions based on the commonly binder-enriched electrodes, the C_S is smaller than those nanosheets synthesized by electrodeposition.[34, 35] But it is bigger than Co_3O_4 synthesized by hydrothermal[26, 56] and some even directly grown on substrate as current collector[40, 44] because of monodispersed mesoporous nanosheets. Thus these results demonstrate that as-prepared mesoporous Co_3O_4 nanosheets have potential applications as electrode materials for supercapacitors.

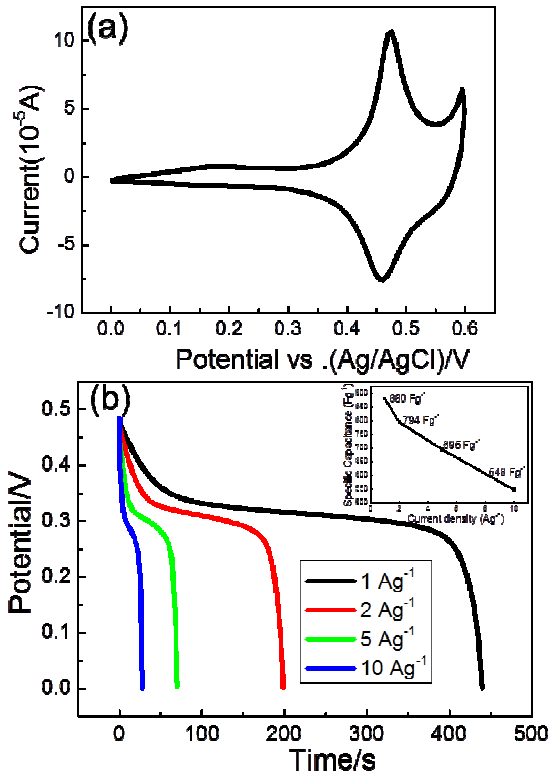

Fig. 11 (a) The CV data of mesoporous Co_3O_4 nanosheets in 1 M KOH aqueous solution at scan rates 20 mV s^{-1} with respect to Ag/AgCl reference electrode; (b) The first discharge curves of mesoporous Co_3O_4 nanosheets electrode at different current densities in 1 M KOH aqueous solution; (inset) specific capacitance of nanosheets Co_3O_4 versus current density.

4. Conclusions

In summary, mesoporous Co_3O_4 nanosheets (about 15 nm in thickness and 1 μm in width) with mostly pore size of 10 ~ 15 nm have been fabricated through a simple hydrothermal process substrate-free along with subsequent heat treatment. Their BET surface area is about 65 m^2g^{-1}. The effects of varying hydrothermal temperature, time and solvent on hydrothermal products' structural, morphological, and compositional

were investigated. In a typical hydrothermal process, $Co(OH)_2$ favors to form at low temperature (120 °C) in dynamics because of high OH^- concentration. And due to NH_4^+ and other ions in solution preferred to adsorb on the special facets of $Co(OH)_2$, it tends to form quasi-sheet-like through the oriented attachment and self-assembly during growth process. However, $Co(OH)_2$ was a thermaldynamic instablity phase and favored to transform to slice sheets $Co(NH_3)_5(ONO)(NO_3)_2$ and $Co(CN)_2 \cdot H_2O$ when temperature increased up to over 150 °C. Their sheets become thinner and more decentralized with the extension of hydrothermal reaction time. And hierarchical nanoflowers-like consisted of $(CH_3COO)_2Co$ petals (sheet-like) were obtained when ethanol instead of water as a solvent. All of hydrothermal products were transformed into porous Co_3O_4 with similar morphologies after heat treatment. Preliminary results of capacitive characteristics clarify mesoporous Co_3O_4 nanosheets show good symmetry and reversibility and the C_S is 880 Fg^{-1} at the discharge current density of 1 Ag^{-1}. The designed Co_3O_4 structures have potential applications in supercapacitors and catalytic field.

Acknowledgments

This work was supported by Program for New Century Excellent Talents in University (NCET-12-0733, China), Specially-Appointed Professors by Universities in Jiangsu Province (SPUJP-2012, China), the National Natural Science Foundation of China (Grant No.51372113), the scientific research foundation for Returned Overseas Students, and Project Funded by the Priority Academic Program Development of Jiangsu Higher Education Institutions (PAPD).

Notes and references

1. Y. Lv, Y. Li and W. Shen, *Catalysis Communications*, 2013, **42**, 116-120.
2. X. Xie, Y. Li, Z.-Q. Liu, M. Haruta and W. Shen, *Nature*, 2009, **458**, 746-749.
3. Y. Lou, L. Wang, Z. Zhao, Y. Zhang, Z. Zhang, G. Lu, Y. Guo and Y. Guo, *Applied Catalysis B-Environmental*, 2014, **146**, 43-49.
4. K. Cheng, D. Cao, F. Yang, Y. Xu, G. Sun, K. Ye, J. Yin and G. Wang, *Journal of Power Sources*, 2014, **253**, 214-223.
5. J. Mu, L. Zhang, M. Zhao and Y. Wang, *Journal of Molecular Catalysis a-Chemical*, 2013, **378**, 30-37.
6. M. T. Makhlouf, B. M. Abu-Zied and T. H. Mansoure, *Applied Surface Science*, 2013, **274**, 45-52.
7. X. Wang, M. Li, Z. Chang, Y. Yang, Y. Wu and X. Liu, *ACS applied materials & interfaces*, 2015, **7**, 2280-2285.
8. F. Su, X. Lv and M. Miao, *Small*, 2015, **11**, 854-861.
9. R. Silva, G. M. Pereira, D. Voiry, M. Chhowalla and T. Asefa, *Rsc Advances*, 2015, **5**, 49385-49391.
10. L. Leng, X. Zeng, H. Song, T. Shu, H. Wang and S. Liao, *Journal of Materials Chemistry A*, 2015, **3**, 15626-15632.
11. G. G. Kumar, M. Christy, H. Jang and K. S. Nahm, *Journal of Power Sources*, 2015, **288**, 451-460.
12. J. Cao, S. Liu, J. Xie, S. Zhang, G. Cao and X. Zhao, *Acs Catalysis*, 2015, **5**, 241-245.
13. X. Zhang, Y. Hou, W. He, G. Yang, J. Cui, S. Liu, X. Song and Z. Huang, *Nanoscale*, 2015, **7**, 3356-3372.
14. M. Zhang, R. Li, X. Chang, C. Xue and X. Gou, *Journal of Power Sources*, 2015, **290**, 25-34.
15. D. Wang, Y. Yu, H. He, J. Wang, W. Zhou and H. D. Abruna, *Acs Nano*, 2015, **9**, 1775-1781.
16. X. Xie and W. Shen, *Nanoscale*, 2009, **1**, 50-60.
17. Y. Lu, W. Zhan, Y. He, Y. Wang, X. Kong, Q. Kuang, Z. Xie and L. Zheng, *ACS applied materials & interfaces*, 2014, **6**, 4186-4195.
18. S. Sadasivan, R. M. Bellabarba and R. P. Tooze, *Nanoscale*, 2013, **5**, 11139-11146.
19. M. Luo, Y. Liu, J. Hu, J. Li, J. Liu and R. M. Richards, *Applied Catalysis B: Environmental*, 2012, **125**, 180-188.
20. S. N. Karthick, K. V. Hemalatha, C. J. Raj, H. J. Kim and M. Yi, *Journal of Nanoparticle Research*, 2013, **15**.
21. J.-H. Shim, S.-W. Cho, A. Missiul, H.-O. Jung and S. Lee, *Journal of Power Sources*, 2015, **274**, 659-666.
22. N. M. Hosny, *Materials Chemistry and Physics*, 2014, **144**, 247-251.
23. S. Farhadi, K. Pourzare and S. Sadeghinejad, *Polyhedron*, 2014, **67**, 104-110.
24. C. Liang, D. Cheng, S. Ding, P. Zhao, M. Zhao, X. Song and F. Wang, *Journal of Power Sources*, 2014, **251**, 351-356.
25. C. Wen, D. Dunbar, X. Zhang, J. Lauterbach and J. Hattrick-Simpers, *Chemical communications (Cambridge, England)*, 2014, **50**, 4575-4578.
26. W. Liu, L. Xu, D. Jiang, J. Qian, Q. Liu, X. Yang and K. Wang, *Crystengcomm*, 2014, **16**, 2395-2403.
27. S. Sharma, N. Garg, K. V. Ramanujachary, S. E. Lofland and A. K. Ganguli, *Crystal Growth & Design*, 2012, **12**, 4202-4210.
28. K. S. Hui, K. N. Hui, C.-L. Yin and X. Hong, *Materials Letters*, 2013, **97**, 154-157.
29. Y. Zhu, W. Chen, C. Nan, Q. Peng, R. Wang and Y. Li, *Crystal Growth & Design*, 2011, **11**, 4406-4412.
30. C. Guan, X. Qian, X. Wang, Y. Cao, Q. Zhang, A. Li and J. Wang, *Nanotechnology*, 2015, **26**.

31. Y.-G. Lu, Y. Li, N. Ta and W.-J. Shen, *Acta Physico-Chimica Sinica*, 2014, **30**, 382-388.
32. J. H. Yang and T. Sasaki, *Crystal Growth & Design*, 2010, **10**, 1233-1236.
33. Y. Fan, H. Shao, J. Wang, L. Liu, J. Zhang and C. Cao, *Chemical communications*, 2011, **47**, 3469-3471.
34. F. Fang, L. Bai, Y. Liu, S. Cheng and H. Sun, *Materials Letters*, 2014, **125**, 103-106.
35. C.-W. Kung, H.-W. Chen, C.-Y. Lin, R. Vittal and K.-C. Ho, *Journal of Power Sources*, 2012, **214**, 91-99.
36. Q. Yang, Z. Lu, X. Sun and J. Liu, *Scientific Reports*, 2013, **3**.
37. X. Wang, H. Guan, S. Chen, H. Li, T. Zhai, D. Tang, Y. Bando and D. Golberg, *Chemical communications*, 2011, **47**, 12280-12282.
38. J. Q. Hu, X. M. Feng, Z. W. Chen and X. H. Chen, *Rare Metal Materials and Engineering*, 2009, **38**, 1026-1029.
39. C. Yuan, L. Yang, L. Hou, L. Shen, F. Zhang, D. Li and X. Zhang, *Journal of Materials Chemistry*, 2011, **21**, 18183-18185.
40. C. Yuan, L. Yang, L. Hou, J. Li, Y. Sun, X. Zhang, L. Shen, X. Lu, S. Xiong and X. W. Lou, *Advanced Functional Materials*, 2012, **22**, 2560-2566.
41. Y. Xiao, C. Hu and M. Cao, *Journal of Power Sources*, 2014, **247**, 49-56.
42. L. J. Xie, K. X. Li, G. H. Sun, Z. A. Hu, C. X. Lv, J. L. Wang and C. M. Zhang, *Journal of Solid State Electrochemistry*, 2013, **17**, 55-61.
43. A. Q. Pan, Y. P. Wang, W. Xu, Z. W. Nie, S. Q. Liang, Z. M. Nie, C. M. Wang, G. Z. Cao and J. G. Zhang, *Journal of Power Sources*, 2014, **255**, 125-129.
44. Y. Q. Zhang, L. Li, S. J. Shi, Q. Q. Xiong, X. Y. Zhao, X. L. Wang, C. D. Gu and J. P. Tu, *Journal of Power Sources*, 2014, **256**, 200-205.
45. S. Xie, J. Deng, S. Zang, H. Yang, G. Guo, H. Arandiyan and H. Dai, *Journal of Catalysis*, 2015, **322**, 38-48.
46. Y. Zhang, X. Zhang, X. Zhang, G. Yue and D. Peng, *Materials Letters*, 2014, **115**, 222-225.
47. C. Yuan, L. Zhang, L. Hou, G. Pang and W.-C. Oh, *Rsc Advances*, 2014, **4**, 14408-14413.
48. W. Liu, D. Jiang, J. X. Xia, J. Qian, K. Wang and H. M. Li, *Monatshefte Fur Chemie*, 2014, **145**, 19-22.
49. X. Zhang, Y. Zhao and C. Xu, *Nanoscale*, 2014, **6**, 3638-3646.
50. G. Huang, S. Xu, S. Lu, L. Li and H. Sun, *ACS applied materials & interfaces*, 2014, **6**, 7236-7243.
51. X. Hu, X. Shen, R. Huang, Y. Masuda, T. Ohji and K. Kato, *Journal of Alloys and Compounds*, 2013, **580**, 373-376.
52. R. B. Rakhi, W. Chen, M. N. Hedhili, D. Cha and H. N. Alshareef, *ACS applied materials & interfaces*, 2014, **6**, 4196-4206.
53. F. Zhan, B. Geng and Y. Guo, *Chemistry-a European Journal*, 2009, **15**, 6169-6174.
54. Y. Lv, Y. Li, N. Ta and W. Shen, *Science China-Chemistry*, 2014, **57**, 873-880.
55. Z.-g. Zhao and M. Miyauchi, *Chemical communications*, 2009, DOI: 10.1039/b823346b, 2204-2206.
56. D. T. Dam and J.-M. Lee, *ACS applied materials & interfaces*, 2014, **6**, 20729-20737.

Graphical Abstract

Controllable Hydrothermal-assisted Synthesis of Mesoporous Co_3O_4 Nanosheets

Xiulan Hu, Huihong Huang, Jianbo Zhang, Junjun Shi, Shoufeng Zhu, Nan Su

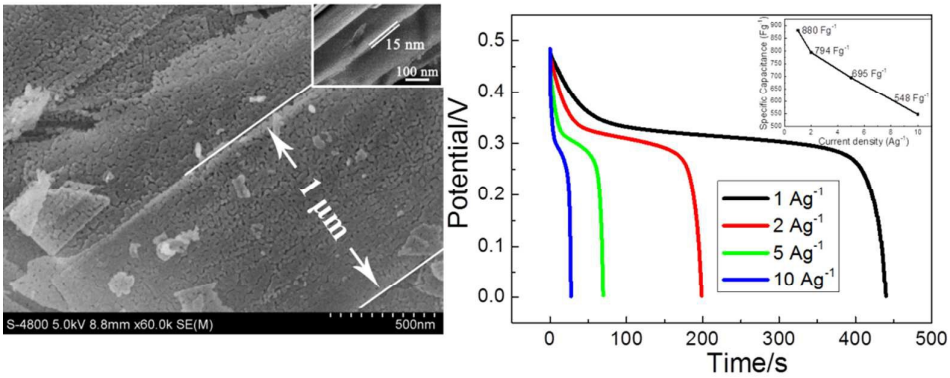

Mesoporous Co_3O_4 nanosheets (about 15 nm in thickness and 1 μm in width) with average pore size of 10 ~ 15 nm were fabricated through a simple hydrothermal process along with subsequent heat treatment. The results of capacitive characteristics clarify the designed mesoporous Co_3O_4 nanosheets have potential applications in supercapacitors.